Research Square

Preprints are preliminary reports that have not undergone peer review.
They should not be considered conclusive, used to inform clinical practice,
or referenced by the media as validated information.

AlGaN/GaN heterojunction field effect transistor structure integrated photoelectrode probe with optical artifact suppression function

Xin Cao
Sun Yat-sen University
Yanyuan Ding
Sun Yat-sen University
Xi'en Yang
Sun Yat-sen University
Wenbo Zhao
Sun Yat-sen University
Xiaodong Li
Sun Yat-sen University
Ye Wen
Sun Yat-sen University
Yang Li
Sun Yat-sen University
Xilei Huang
Sun Yat-sen University
Zeyi Li
Sun Yat-sen University
Jiefeng Weng
Sun Yat-sen University
Baijun Zhang
zhbaij@mail.sysu.edu.cn
Sun Yat-sen University

Research Article

Keywords: AlGaN/GaN heterostructure field-effect transistor, Brain neural probe, Integrated photoelectrode probe, Optical artifacts, Optogenetics

Posted Date: July 3rd, 2026

DOI: https://doi.org/10.21203/rs.3.rs-10147214/v1

License: This work is licensed under a Creative Commons Attribution 4.0 International License.
Read Full License

Additional Declarations: No competing interests reported.

Version of Record: A version of this preprint was published at Biomedical Microdevices on September 18th, 2026. See the published version at https://doi.org/10.1007/s10544-026-00851-9.

AlGaN/GaN heterojunction field effect transistor structure integrated photoelectrode probe with optical artifact suppression function

Xin Cao†, Yanyuan Ding†, Xi'en Yang, Wenbo Zhao, Xiaodong Li, Ye Wen, Yang Li, Xilei Huang, ZeYi Li, Jiefeng Weng, Baijun Zhang*

State Key Laboratory of Optoelectronic Materials and Technologies, Sun Yat-sen University, Guangzhou, 510006, China.

Contributing authors: caox58@mail2.sysu.edu.cn; dingyy27@mail2.sysu.edu.cn; yangxen@mail2.sysu.edu.cn; zhaowb27@mail2.sysu.edu.cn; lixd65@mail2.sysu.edu.cn; weny87@mail2.sysu.edu.cn; liyang325@mail2.sysu.edu.cn; huangxlei@mail2.sysu.edu.cn; lizy298@mail2.sysu.edu.cn; wengjf3@mail2.sysu.edu.cn; zhbaij@mail.sysu.edu.cn;

†These authors contributed equally to this work.

Abstract

The integrated photoelectrode probe capable of simultaneously stimulating neurons with light and collecting electrophysiological signals is the core device of optogenetics. In this paper, AlGaN/GaN heterojunction field-effect transistors (HFETs) are used instead of the traditional metal microelectrode to prepare brain neural probe, and then bonded with the LED photoelectrode probe to form an integrated photoelectrode probe. The AlGaN/GaN HFET structure brain neural probe has high sensitivity and biocompatibility, which can effectively improve the quality of neuronal signal acquisition. While the light stimulation signal of the LED photoelectrode probe will affect the AlGaN/GaN HFET, severely degrading the signal-to-noise ratio (SNR) of neuronal signal acquisition. We prepared multiple pairs of recording HFET (R-HFET) and differential HFET (D-HFET) at the tip of the brain nerve probe. The R-HFET has a bare gate region that is sensitive to changes in extracellular potential and is used for collecting neuronal signals. The gate region of D-HFET is covered with a SiO_2 passivation film, which has low sensitivity to changes in extracellular potential

and can hardly collect neuronal signals. D-HFET, like R-HFET, is sensitive to the light stimulation signal from the LED photoelectrode probe. By adjusting the drain-source bias of D-HFET and performing differential processing with the signal collected by R-HFET, the neuronal signal can be clearly separated. Simulated biological experiments in phosphate buffered saline solution have shown that the integrated photoelectrode probe can reduce artifacts by 90%.

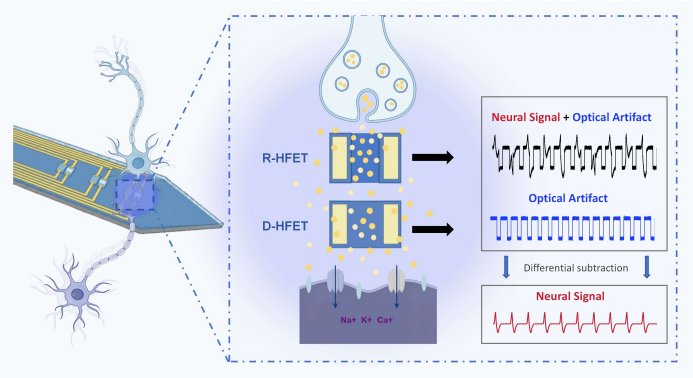


Fig. 1 Graphical Abstract

Keywords: AlGaN/GaN heterostructure field-effect transistor, Brain neural probe, Integrated photoelectrode probe, Optical artifacts, Optogenetics

1 Introduction

Simultaneous optical stimulation and electrical recording links neural perturbations to electrophysiological responses with high precision.[1–3] Conventional passive metal electrodes often suffer from parasitic feedthrough and photoelectrochemical noise during these experiments.[4, 5] In contrast, AlGaN/GaN recording heterojunction field-effect transistor (R-HFET) provide active sensing through field-effect modulation. The device offers intrinsic transconductance amplification, strong electromagnetic interference resistance, and high signal-to-noise ratios.[6–8] However, the illumination required to activate photosensitive proteins introduces severe optical artifacts in AlGaN/GaN devices. Although GaN possesses a wide band gap, sub-bandgap optical transitions still generate internal photocarriers.[9, 10] These light-induced current transients often exceed the amplitude of weak neural signals. Consequently, intense optical artifacts can distort target readouts and severely degrade the overall signal-to-noise ratio.[11] Maintaining the exceptional sensitivity of R-HFET while suppressing these optical artifacts remains a critical bottleneck.

Previous efforts to resolve this issue have largely focused on surface passivation and interface engineering. For example, depositing high-quality SiN_x or Al_2O_3 layers mitigates defect-mediated charge trapping.[12–14] These treatments effectively suppress persistent photoconductivity and transient artifacts caused by trap states. Nevertheless, these interface modifications introduce fundamental trade-offs for neural recording applications. The AlGaN barrier layer serves as the primary sensing region for detecting extracellular potentials. Depositing additional materials over this region physically impedes ionic coupling, directly reducing detection sensitivity. Furthermore, surface engineering inherently shifts the threshold voltage of the transistor.[15, 16] This shift moves the optimal transconductance operating point away from a zero gate bias.[17, 18] An urgent need therefore exists for a readily integrable artifact suppression approach that preserves the high intrinsic sensitivity of the device.

Here, we demonstrate a drain-source bias-tuned differential AlGaN/GaN integrated photoelectrode probe to address this gap. The architecture pairs a recording R-HFET with a co-fabricated differential HFET (D-HFET) on a single chip. The R-HFET gate remains exposed to the electrolyte, allowing local solution-potential fluctuations to modulate conductance. Conversely, a dense passivation layer completely covers the D-HFET gate. This passivation effectively suppresses solution-potential sensitivity while entirely preserving the semiconductor optical response. By adjusting the drain-source bias of the D-HFET, we matched its photocurrent to the R-HFET. Subtracting this matched reference output efficiently cancels the shared optical interference. During simulated recording under strong illumination, this differential readout suppressed optical artifacts by up to 90%. The approach successfully recovered weak neural-like waveforms that were completely obscured in the direct trace. Importantly, this differential design provides a versatile framework for rejecting other common-mode environmental interferences.

2 Experimental Section

2.1 Differential probe architecture and operating principle

The AlGaN/GaN heterojunction neural probe contains co-fabricated R-HFET and D-HFET sensing sites on the same chip, as illustrated in Fig.2(a-d). Both devices share the identical epitaxial platform and packaging route but differ at the gate interface. The R-HFET gate region is selectively opened to the electrolyte, so that local solution-potential changes modulate the two-dimensional electron gas (2DEG) and are converted into drain-source current variations. In contrast, the D-HFET gate remains covered by a dense SiO_2 passivation layer. This structural asymmetry enables the R-HFET to function as the recording transistor and the D-HFET to serve as a local optical reference.

This configuration separates the electrical and optical roles of the two devices. In a recording scenario, extracellular potential changes are expected to couple primarily into the R-HFET channel, whereas the passivated D-HFET is designed to reject those solution-potential variations. Because the two devices are co-fabricated and closely co-localized, they experience similar material, packaging, and illumination environments

after optical integration. This arrangement provides the physical basis for common-mode optical-artifact subtraction.

2.2 Probe fabrication and optical integration

The AlGaN/GaN heterojunction probes were fabricated from metal-organic chemical vapor deposition (MOCVD)-grown AlGaN/GaN HEMT epitaxial wafers on sapphire substrates. Wafers were sequentially cleaned with SPM solution, acetone, isopropanol, and deionized water to remove particulates, native oxides, and organic residues. Mesa isolation was performed by inductively coupled plasma (ICP) etching to interrupt the 2DEG in passive regions and electrically isolate adjacent devices. Probe outlines were then defined lithographically and transferred by deep ICP etching down to the sapphire substrate.

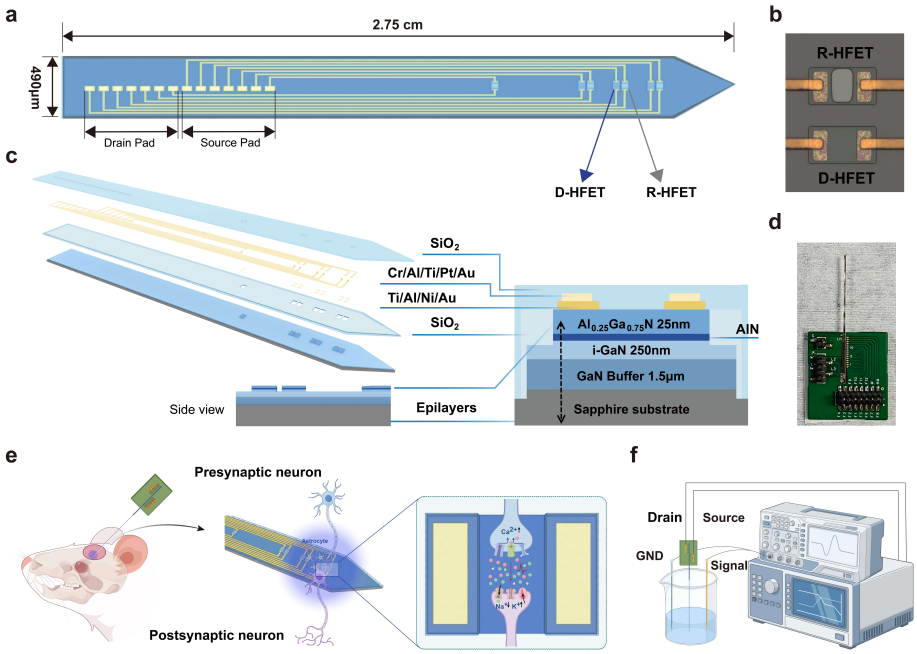


Fig. 2 Architecture, fabrication, and sensing principle of the AlGaN/GaN heterojunction neural probe. a, Top view of the heterojunction neural probe. b, Optical micrographs of the R-HFET and D-HFET. c, Layer structure of the AlGaN/GaN device. d, Packaged probe on a custom PCB. e, Sensing principle during electrical recording. f, Saline-based test platform for controlled injection of a neural-like signal.

A 200 nm insulating layer was deposited in passive regions by plasma-enhanced chemical vapor deposition (PECVD) to suppress leakage-current paths. Ti/Al/Ni/Au (15/80/20/60 nm) ohmic-contact stacks were formed by electron-beam evaporation (EBE) and rapid thermal annealing for 30 s in a nitrogen atmosphere. Cr/Al/Ti/Pt/Au metallization was deposited to define interconnects and bonding pads, followed

by a thick SiO_2 passivation layer. Buffered oxide etchant was used for selective wet etching to open windows only over the R-HFET gate and pad regions, while the D-HFET gate remained fully covered. This selective passivation established the functional distinction between the solution-sensitive R-HFET and the passivated reference D-HFET.

After front-side processing, wafers were thinned by mechanical grinding and chemical mechanical polishing, then diced along the probe scribe lanes by laser stealth dicing and mechanical separation. Individual probes were mounted on custom printed-circuit-board adapters, and aluminum ultrasonic wire bonding connected the chip pads to the adapter contacts for characterization.

2.3 Electrical measurement and data processing

The intended recording principle in an optogenetic experiment is illustrated in Fig. 2(e): extracellular potential changes at the biointerface are transduced by the R-HFET. Direct biological measurements, however, can introduce additional variables such as tissue-probe coupling, spontaneous activity, motion artifacts, and time-dependent interfacial drift. Therefore, before proceeding to biological preparations, a simplified in vitro platform was employed as a controlled pre-biological validation step to quantitatively evaluate the probe's ability to detect weak electrophysiological-scale signals and suppress optical artifacts. The saline-based test platform is shown in Fig.2(f). PBS was used as a defined ionic medium, and a weak neural-like waveform generated by an arbitrary waveform generator was attenuated to a physiological amplitude range and delivered into the saline through a gold probe positioned near the sensing region. During measurement, the bath was grounded while drain-source current was recorded with a Keysight B1500A semiconductor parameter analyzer. This platform enabled electrical sensitivity, reference-channel rejection, and optical-artifact suppression to be evaluated without uncontrolled biological variability.

The differential signal was calculated from the simultaneously recorded R-HFET and D-HFET currents after baseline correction:

$$I_{\mathrm{Diff}} = I_{\mathrm{DS\ R-HFET}} - I_{\mathrm{DS\ D-HFET}} \tag{1}$$

where the D-HFET drain-source bias was adjusted to match the transient optical response of the R-HFET. The optical-artifact suppression ratio was defined as

$$\mathrm{Suppression} = \left(1 - \frac{I_{\mathrm{Diff}}}{I_{\mathrm{DS\ R-HFET}}}\right) \times 100\% \tag{2}$$

where $I_{\mathrm{DS\ R-HFET}}$ and I_{Diff} are the peak-to-peak artifact amplitudes in the RHFET and differential traces, respectively, calculated over the same illumination window after pre-pulse baseline subtraction. The signal-to-noise ratio was calculated as

$$\mathrm{SNR} = 20 \log_{10}\left(\frac{I_{\mathrm{signal,rms}}}{I_{\mathrm{noise,rms}}}\right) \tag{3}$$

using identical analysis windows for direct and differential recordings.

3 Results and Discussion

3.1 Electrical characteristics and functional separation

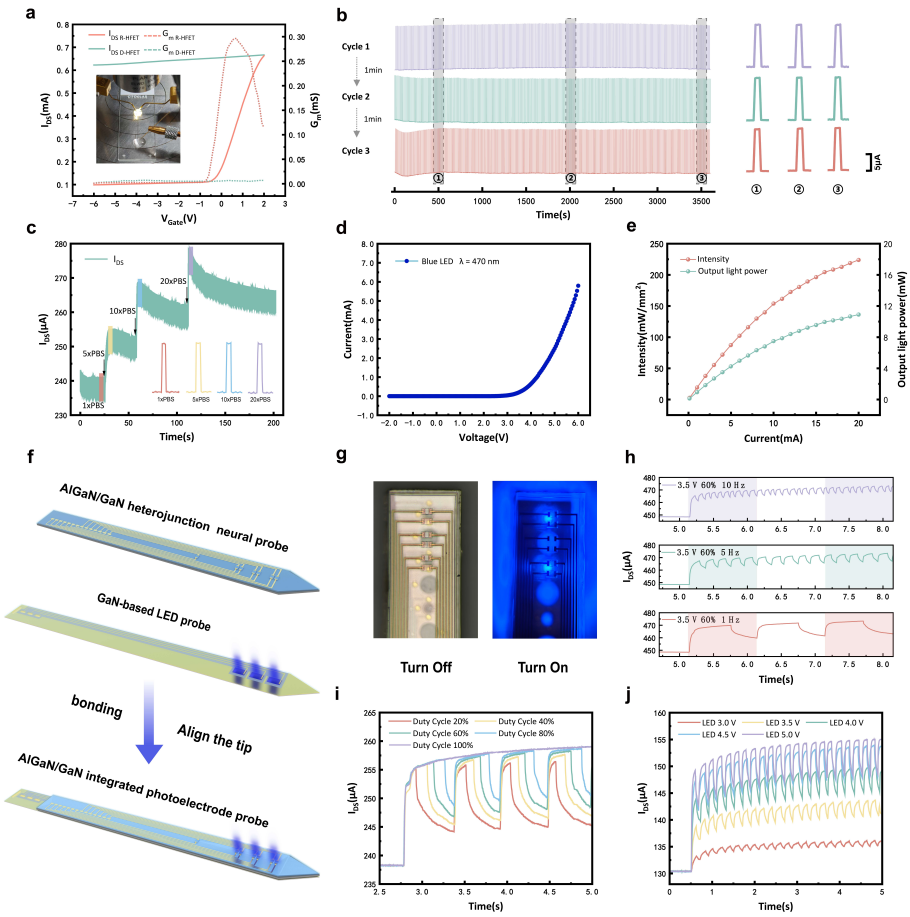


Fig. 3 Electrical characterization and optical integration of differential AlGaN/GaN integrated photoelectrode probes. a, Transfer characteristics and transconductance of the R-HFET and D-HFET in PBS. b, Repeated 1 h cycle tests. c, Response to PBS concentration perturbations. d, Current-voltage characteristics of the integrated blue LED. e, Optical output of the LED. f-g, Bonding scheme and photograph of the AlGaN/GaN integrated photoelectrode probe configuration. h-j, Dependence of the R-HFET photoresponse on pulse frequency, duty cycle, and driving voltage.

Electrical characterization in PBS confirmed the intended functional separation between the recording and reference transistors (Fig.3(a-c)). The R-HFET exhibited strong gate modulation with a transconductance reaching approximately 0.25 mS, indicating effective coupling between solution-potential changes and channel current.

In contrast, the D-HFET remained normally on and exhibited negligible transconductance across the tested gate bias range. This behavior is consistent with dielectric screening of the passivated gate region and confirms that the D-HFET does not function as a second solution-potential sensor.

The probe also maintained stable operation under conditions relevant to simulated recording. During three consecutive 1 h measurement cycles, the R-HFET response to the same injected analog waveform remained reproducible and exhibited limited hysteresis. The device was further challenged by perturbing the ionic environment through concentrated PBS additions. Under these conditions, the drain-source current baseline shifted with the electrochemical environment, yet the target waveform remained detectable. Together, these measurements demonstrate that the AlGaN/GaN heterojunction probe combines clear functional separation between R-HFET and D-HFET with stable signal detection in a controlled saline environment.

3.2 Optical integration and photoresponse characterization

Optical characterization (Fig.3(d-e)) confirmed that the integrated blue LED exhibited a turn-on voltage of approximately 2.3 V and delivered adequate optical output at 3.0 V for the measurements reported here. The heterojunction probe was then configured as a differential AlGaN/GaN integrated photoelectrode probe by aligning a sapphire-substrate GaN LED beneath the R-HFET and D-HFET sensing regions through a top-aligned, tail-offset bonding process (Fig.3(f)). In this vertically integrated architecture, the light source and sensing elements occupy the same local footprint. Compared with side-by-side layouts employing opaque metal electrodes, this geometry exploits the optical transparency of the AlGaN/GaN epitaxial stack and sapphire substrate, thereby reducing optical shielding.

After integration, the R-HFET light response exhibited systematic dependence on LED pulse frequency, duty cycle, and driving voltage (Fig.3(h-j)). This systematic dependence confirmed that the integrated probe provides a well-controlled platform for evaluating device-level optical artifacts and their differential suppression.

3.3 Mechanism of the optical artifact and bias-tuned reference matching

We next examined the origin and tunability of the optical response Fig.4(a,b). Under 470 nm blue-light excitation, the R-HFET transfer characteristics shifted upward and leftward, corresponding to increased drain-source current and a negative shift in threshold voltage at a given gate bias. Because the photon energy is below the GaN band gap, the response is consistent with sub-bandgap transitions mediated by defect states in the epitaxial stack. In this interpretation, illumination releases trapped carriers, restores part of the channel carrier concentration, and increases the measured current.

The optical artifact was therefore treated as a reproducible device response rather than a random disturbance. This interpretation was supported by the monotonic relationship between LED driving voltage and R-HFET drain-source current. Over the tested operating range, the R-HFET photocurrent increased approximately linearly

with LED bias, consistent with a controllable optical component that can be matched and subtracted.

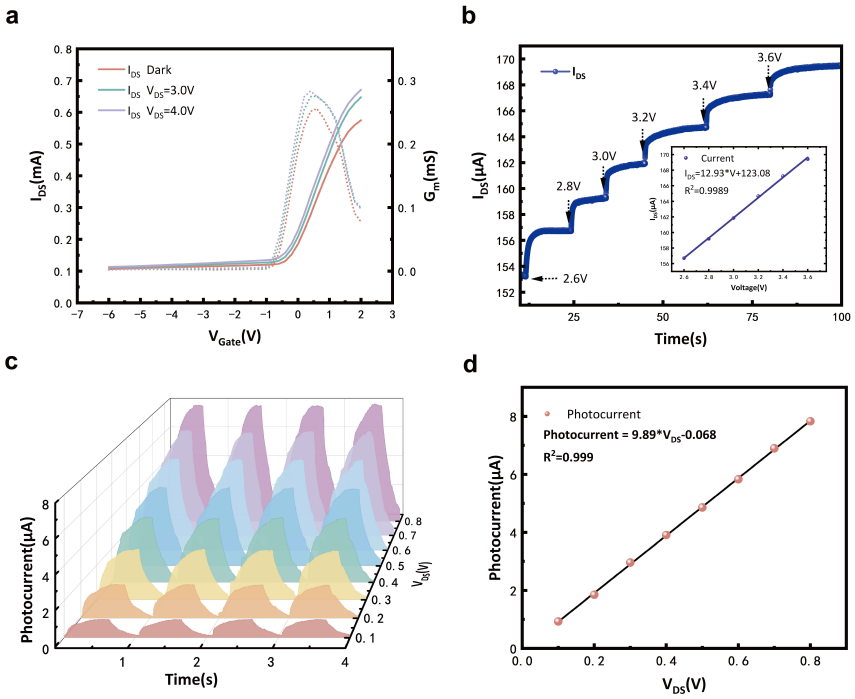


Fig. 4 Optical response of the R-HFET and bias-dependent tuning of the D-HFET reference. a, R-HFET transfer characteristics in the dark and under increasing LED drive. b, Relationship between LED bias and R-HFET photocurrent. c, D-HFET photocurrent at different drain-source biases under fixed illumination. d, Approximate linear relationship between D-HFET bias and photocurrent, enabling response matching.

The D-HFET provided a practical route for reference matching. Under fixed illumination, the D-HFET photocurrent increased approximately linearly as the drain-source bias was raised Fig.4(c-d). Under a simplified photoconductive-gain description, the measured photocurrent can be written as

$$I_{\mathrm{ph}} = \eta q \Phi G \tag{4}$$

where η is the internal quantum efficiency, Φ is the incident photon flux, q is the elementary charge, and G is the photoconductive gain. The gain can be expressed as the ratio between the photogenerated carrier lifetime τ and the carrier transit time t_{tr}:

$$G = \frac{\tau}{t_{\mathrm{tr}}} \tag{5}$$

with the transit time approximated as

$$t_{\mathrm{tr}} = \frac{L^2}{\mu V_{\mathrm{DS}}} \tag{6}$$

where L and μ denote the channel length and carrier mobility, respectively. These relations predict an approximately linear dependence of I_{ph} on V_{DS} under fixed illumination, consistent with the experimental trend in Fig.4d. The empirical bias dependence, rather than the model alone, was used to tune the DHFET response toward the RHFET optical artifact.

This tunability is central to the differential strategy. The D-HFET does not merely report the presence of illumination; it provides a bias-adjustable optical reference whose transient amplitude can be matched to that of the R-HFET while maintaining low sensitivity to solution-potential changes. Response matching, rather than baseline alignment alone, is therefore the key condition for effective common-mode subtraction.

3.4 Differential suppression of optical artifacts

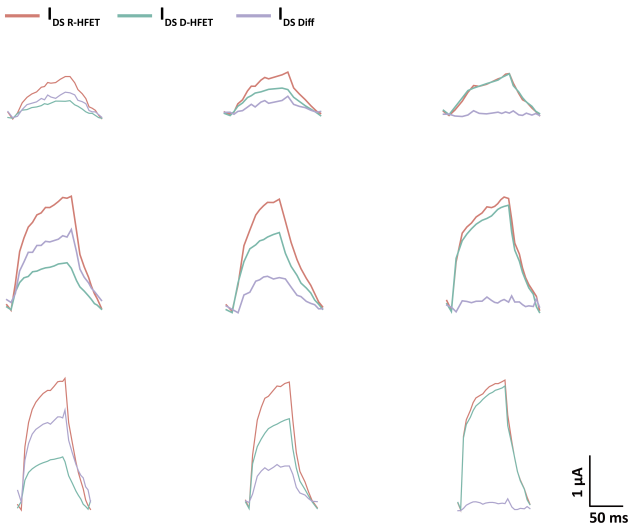


Fig. 5 Drain-source bias-tuned differential subtraction suppresses optical artifacts across illumination conditions. Differential traces were recorded at three optical power densities and several D-HFET drain-source biases. Rows correspond to 5, 20, and 65 mW mm^{-2} illumination, and columns correspond to representative D-HFET biases of 0.18, 0.30, and 0.40 V. Optimal suppression occurred when the D-HFET transient matched the R-HFET optical response.

The D-HFET was used as an on-chip reference to test whether common-mode optical current could be cancelled by differential subtraction Fig.5. Measurements were collected at optical power densities of 5, 20, and 65 mW mm^{-2} while the D-HFET drain-source bias was varied from 0.18 to 0.40 V. Both R-HFET and D-HFET

photocurrent amplitudes increased with illumination intensity, indicating that the two devices sampled the same local optical perturbation.

The importance of bias tuning became apparent when the dynamic amplitudes of the two devices were compared. At low D-HFET bias, the static baselines of the R-HFET and D-HFET could be brought close to one another, but the transient light response of the D-HFET remained too small. Differential subtraction under these conditions removed only part of the interference and left a residual optical artifact. As the D-HFET bias increased, its photoconductive gain increased, and the transient response approached that of the R-HFET. This intermediate regime shows that artifact suppression is governed by transient response matching rather than simple baseline cancellation.

When the D-HFET bias reached approximately 0.40 V, the light-induced transients of the R-HFET and D-HFET were closely matched, and the differential output showed the strongest suppression of common-mode interference. Under these conditions, the artifact suppression ratio reached up to approximately 90%. This suppression was achieved without additional shielding layers, recording blanking, or post-acquisition filtering to recover a saturated trace. These results support co-fabricated reference subtraction as a device-level route for reducing optical artifacts in AlGaN/GaN integrated photoelectrode probes.

3.5 Recovery of neural-like waveforms under illumination

We next evaluated whether the integrated photoelectrode probe could preserve weak neural-like waveforms during concurrent illumination Fig.6. Under dark conditions, the R-HFET detected the injected analog signal in PBS with an SNR of 22.9 dB. The D-HFET showed no obvious response to the same waveform, consistent with suppression of solution-potential coupling by the passivated gate. After differential processing, the recovered signal exhibited an SNR of 22.3 dB, indicating that the reference path did not materially degrade signal quality under dark conditions.

When the 470 nm LED was operated at an optical power density of 5 mW mm^{-2}, the R-HFET trace became dominated by a large light-induced current, and the weak neural-like waveform was no longer directly readable. The D-HFET primarily reported the shared optical perturbation and did not carry the injected waveform. Subtracting the D-HFET current from the R-HFET current removed much of the common-mode component and recovered the analog waveform with an SNR of 21.8 dB. During the post-illumination relaxation period, carrier recombination produced a residual decay component, but the system maintained an SNR of 22.7 dB after light turn-off.

At a higher optical power density of 20 mW mm^{-2}, the injected waveform became effectively obscured in the direct R-HFET output. Even under this stronger interference condition, differential readout reconstructed the waveform with a final SNR of 16.9 dB. Within the controlled PBS model used here, these measurements show that bias-matched differential readout can preserve weak neural-like signals under illumination conditions that obscure direct R-HFET recording.

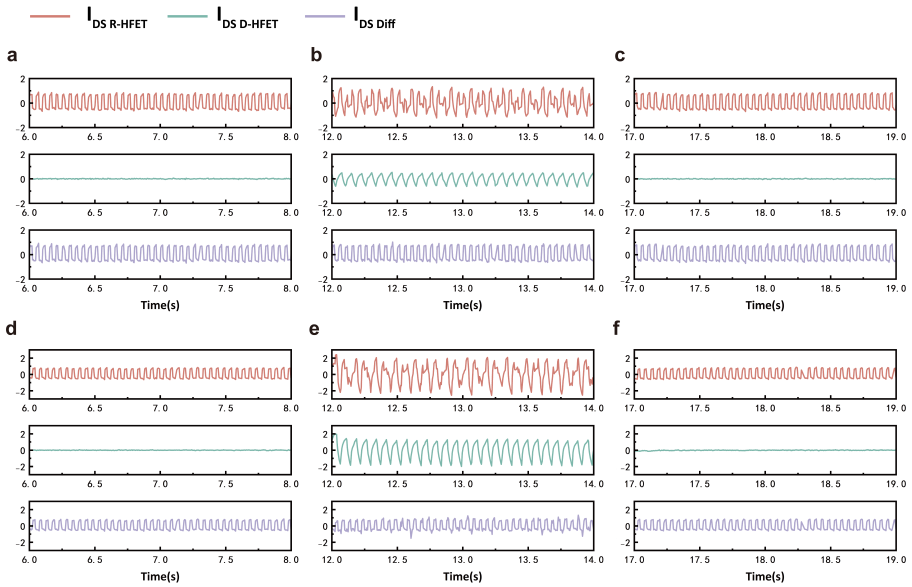


Fig. 6 Differential readout suppresses optical artifacts and recovers weak neural-like signals in a saline model. Representative R-HFET, D-HFET, and differential traces were recorded in a saline-based platform under dark conditions and during concurrent blue-light illumination. Under dark conditions, differential processing preserved baseline signal quality. At 5 and 20 mW mm^{-2}, the differential output recovered the injected waveform.

4 Conclusion

This work presents an AlGaN/GaN integrated photoelectrode probe that suppresses optical artifacts through a drain-source bias-tuned differential strategy. The probe employs AlGaN/GaN HFETs in place of conventional passive metal microelectrodes, leveraging the intrinsic transconductance amplification and high sensitivity of the HFET to enhance neuronal signal acquisition. Its architecture pairs a solution-sensitive R-HFET with a passivated D-HFET reference on the same chip, the two devices vertically integrated with a blue GaN LED. In a controlled PBS test platform, the R-HFET detected weak neural-like waveforms, while the D-HFET rejected solution-potential signals and provided a bias-tunable optical reference. By matching the D-HFET photocurrent transient to that of the R-HFET, differential subtraction reduced optical artifacts by up to approximately 90% and recovered weak neural-like waveforms that were completely obscured in direct R-HFET recordings. These findings establish bias-tuned differential readout as an effective device-level approach for optical-artifact suppression in AlGaN/GaN bioelectronic probes. Furthermore, this differential strategy provides a versatile framework for rejecting other common-mode environmental disturbances, broadening its applicability in optogenetic research.

Acknowledgements. This work was supported by the joint funding of the Nature Science Foundation of China (NSFC) and the Macao Science and Technology Development Fund (FDCT) of China (grantnos. 62061160368 and 0022/2020/AFJ).

Declarations

- Funding
  This work was supported by the joint funding of the Nature Science Foundation of China (NSFC) and the Macao Science and Technology Development Fund (FDCT) of China (grantnos. 62061160368 and 0022/2020/AFJ).
- Conflict of interest/Competing interests (check journal-specific guidelines for which heading to use)
  The authors declare no competing interests.
- Ethics approval and consent to participate
  Not applicable
- Consent for publication
  Not applicable.
- Data availability
  The data that support the findings of this study are available from the corresponding author upon reasonable request.
- Materials availability
  Not applicable.
- Code availability
  Not applicable.
- Author contribution
  Conceptualization: Xin Cao, Yanyuan Ding, Baijun Zhang;
  Methodology: Xin Cao, Yanyuan Ding, Xi'en Yang;
  Investigation: Yanyuan Ding, Wenbo Zhao, Xiaodong Li, Ye Wen, Yang Li, Xilei Huang, ZeYi Li, Jiefeng Weng;
  Writing - Original Draft: Xin Cao;
  Writing - Review & Editing: Xin Cao, Baijun Zhang;
  Supervision: Baijun Zhang;
  All authors have read and agreed to the published version of the manuscript.

References

[1] Alifragis, Y., Volosirakis, A., Chaniotakis, N., Konstantinidis, G., Adikimenakis, A., Georgakilas, A.: Potassium selective chemically modified field effect transistors based on algan/gan two-dimensional electron gas heterostructures. Biosensors and Bioelectronics **22**(12), 2796–2801 (2007)

[2] Anikeeva, P., Andalman, A.S., Witten, I., Warden, M., Goshen, I., Grosenick, L., Gunaydin, L.A., Frank, L.M., Deisseroth, K.: Optetrode: a multichannel readout for optogenetic control in freely moving mice. Nature Neuroscience **15**(1), 163–170 (2012)

[3] Aravanis, A.M., Wang, L.-P., Zhang, F., Meltzer, L.A., Mogri, M.Z., Schneider, M.B., Deisseroth, K.: An optical neural interface: in vivo control of rodent motor cortex with integrated fiberoptic and optogenetic technology. Journal of Neural Engineering **4**(3), 143–156 (2007)

[4] Fenno, L., Yizhar, O., Deisseroth, K.: The development and application of optogenetics. Annual Review of Neuroscience **34**(2011), 389–412 (2011)

[5] Gu, Z., Wang, J., Miao, B., Zhao, L., Liu, X., Wu, D., Li, J.: Highly sensitive algan/gan hemt biosensors using an ethanolamine modification strategy for bioassay applications. RSC Advances **9**(27), 15341–15349 (2019)

[6] Sarangadharan, I., Regmi, A., Chen, Y.-W., Hsu, C.-P., Chen, P.-c., Chang, W.-H., Lee, G.-Y., Chyi, J.-I., Shiesh, S.-C., Lee, G.-B., *et al.*: High sensitivity cardiac troponin i detection in physiological environment using algan/gan high electron mobility transistor (hemt) biosensors. Biosensors and Bioelectronics **100**, 282–289 (2018)

[7] Shen, J., Xu, Y., Xiao, Z., Liu, Y., Liu, H., Wang, F., Yan, C., Wang, L., Chen, C., Wu, Z., *et al.*: Double-sided sapphire optrodes with conductive shielding layers to reduce optogenetic stimulation artifacts. Micromachines **13**(11), 1836 (2022)

[8] Stutzmann, M., Steinhoff, G., Eickhoff, M., Ambacher, O., Nebel, C., Schalwig, J., Neuberger, R., Müller, G.: Gan-based heterostructures for sensor applications. Diamond and related materials **11**(3-6), 886–891 (2002)

[9] Kang, T.S., Lin, Y.-H., Ahn, S., Ren, F., Gila, B.P., Pearton, S.J., Cheney, D.J.: Identification of trap locations in algan/gan high electron mobility transistors by varying photon flux during sub-bandgap optical pumping. Journal of Vacuum Science & Technology B **34**(1) (2016)

[10] Gunn, A.W., Prio, M.H., Gajula, D., Koley, G.: Sub-bandgap photon-assisted electron trapping and detrapping in algan/gan heterostructure field-effect transistors. Physica Scripta **98**(6), 065808 (2023)

[11] Kozai, T.D., Vazquez, A.L.: Photoelectric artefact from optogenetics and imaging on microelectrodes and bioelectronics: new challenges and opportunities. Journal of Materials Chemistry B **3**(25), 4965–4978 (2015)

[12] Hou, M., So, H., Suria, A.J., Yalamarthy, A.S., Senesky, D.G.: Suppression of persistent photoconductivity in algan/gan ultraviolet photodetectors using in situ heating. IEEE Electron Device Letters **38**(1), 56–59 (2016)

[13] Hashizume, T., Ootomo, S., Hasegawa, H.: Suppression of current collapse in insulated gate algan/gan heterostructure field-effect transistors using ultrathin al 2 o 3 dielectric. Applied Physics Letters **83**(14), 2952–2954 (2003)

[14] Peng, Z., Wu, M., Lv, Z., Yang, S., Song, M., Yin, Y., Jiang, H.: Effective mitigation of persistent photoconductivity in algan solar-blind field-effect phototransistors via in-situ sin x passivation. IEEE Electron Device Letters **45**(11), 2074–2077 (2024)

[15] Tanaka, T., Shiojima, K., Otoki, Y., Tokuda, Y.: A study on multiple defect states in low-carbon doped gan layers and its correlation with algan/gan high electron mobility transistor operation. Thin Solid Films **557**, 207–211 (2014)

[16] Yang, C., Sun, J., Zhang, Y., Tang, J., Liu, Z., Zhan, T., Wang, D.-B., Zhang, G., Liu, Z., Zhang, X.-E.: Construction of algan/gan high-electron-mobility transistor-based biosensor for ultrasensitive detection of sars-cov-2 spike proteins and virions. Biosensors and Bioelectronics **257**, 116171 (2024)

[17] Mistele, D., Katz, O., Horn, A., Bahir, G., Salzman, J.: Engineering and impact of surface states on algan/gan-based hetero field effect transistors. Semiconductor Science and Technology **20**(9), 972–978 (2005)

[18] Turkulets, Y., Shalish, I.: Surface states in algan/gan high electron mobility transistors: Quantitative energetic profiles and dynamics of the surface fermi level. Applied Physics Letters **115**(2) (2019)